

## Vortex Shedding during flow following a Square obstacle – A Computational Fluid Dynamics approach

V. Leela Vinodhan

Centre for Nanotechnology & Advanced Biomaterials (CeNTAB), School of Chemical & Biotechnology, SASTRA University, Thanjavur – 613401, India.

**Abstract:** Two dimensional numerical analysis of vortex shedding during flow following a square obstacle at Reynolds number,  $Re = 2.2 \times 10^4$  with different turbulence models are extensively studied. The unsteady flow features viz., Strouhal number (St), forces acting on the geometry under investigation, turbulent characteristics and flow separation around the square obstacle are captured with various turbulence models. The present study demonstrates that the use of k- $\epsilon$  turbulence model predict better results as compared to other standard turbulence model.

**Keywords:** Vortex shedding, square obstacle, Strouhal number.

### 1. Introduction

Computational fluid dynamics is widely used to simulate momentum and heat transports in complex systems such as multiphase flows [1–6]. Flow around the bluff bodies has drawn attention due to the academic desirability, and the significant practical applications connected with conservation of energy and structural design. In the past three decades, several investigators conducted study on the flow around the bluff bodies to understand the intrinsic change in the flow experimentally and numerically [7–29]. Tamura and Kuwahara [19] studied the flow around a cylindrical body at high Reynolds number, placed in a uniform stream numerically. Significant difference in the result was demonstrated between the 2-D and 3-D analysis, with 3-D analysis closely mimicking the experimental data. Kawamura and Kawashima [11] studied unsteady flow around a square obstacle confined in a channel at  $Re = 2.2 \times 10^4$  and their results were compared with those Lyn et al. [30]. Norberg [14] conducted a study to measure the pressure force with the angle between  $0^\circ$  to  $90^\circ$  around a rectangular cylinder within the range of  $Re = 4.0 \times 10^2$  to  $3.0 \times 10^4$

The effect of the aspect ratio of the bluff body has been studied experimentally by many investigators. The flow visualization of the flow around the rectangular cylinder in the range of  $Re = 2.0 \times 10^4$  to  $7.0 \times 10^4$  was conducted by Bearman and Trueman [7]. Their results gave an insight of the mean drag force, pressure and vortex shedding frequency. Okajima et al. [15] presents the features of the flow around the rectangular cylinders with aspect ratio between 1 to 4 in the range of  $7.0 \times 10^1$  and  $2.0 \times 10^4$ . Rapid transformation in the flow patterns were observed in the aspect ratio of 2 and 3. Raisee et al. [31] simulated the 2-D transient at  $Re = 2.2 \times 10^4$  using Reynolds Averaged Navier Stokes (RANS) turbulence model. Their approach of unsteady evaluation with linear and non linear k- $\epsilon$  model enhances the accuracy of predicting the velocity field. Stein T. Johansen et al. [10] delivers significant results on unsteady RANS computations with filter-based approach. G. Iaccarino et al. [9] studied the unsteady flow around a square obstacle and a cube mounted on the wall. Their results revealed the compatibility of the RANS for periodic shedding prediction. Bosch et al. [32] numerically studied the effect of different turbulence model for vortex shedding flow over a square obstacle at  $Re = 2.2 \times 10^4$ . They included the wall function conditions to the standard k- $\epsilon$  model and compared the results with the modifications recommended by Kato and Launder.

In general, the study of the unsteady flow around the bluff body, especially square obstacle is intricate. The present study is aimed in the direction at the numerical simulation of flow past a square obstacle at  $Re = 2.2 \times 10^4$  with difference turbulence model.

## 2. Mathematical formulation

### 2.1 Governing Equation

For numerical study of flow following a square obstacle 2-D Navier Stokes equations applicable for incompressible fluid. The equations of continuity & momentum are given in the dimensionless form:

$$\frac{\partial \bar{u}_i}{\partial x_i} = 0 \quad (1)$$

$$\frac{\partial \bar{u}_i}{\partial t} + \frac{\partial \bar{u}_i}{\partial x_i} + \bar{u}_j \frac{\partial \bar{u}_i}{\partial x_j} = -\frac{1}{\rho} \frac{\partial \bar{p}}{\partial x_i} + \frac{\partial (\bar{\tau}_{ij} + \tau_{ij}^R)}{\partial x_j} \quad (2)$$

Where,

$$\tau_{ij}^R = -\rho \overline{u_i' u_j'} \quad \text{and} \quad \bar{\tau}_{ij} = \frac{\mu}{\rho} \left( \frac{\partial \bar{u}_i}{\partial x_j} + \frac{\partial \bar{u}_j}{\partial x_i} \right) \quad (3)$$

In the equations above,  $\bar{u}_i$  is the velocity in a specific direction  $x_i$ . Fluid properties,  $\rho$  is fluid density and  $\mu$  is viscosity. The equations for turbulent kinetic energy ( $k$ ) & rate of dissipation ( $\varepsilon$ ) in the differential forms are written as follows [33]:

$$\frac{\partial k}{\partial t} + \frac{\partial [\bar{u}_j k]}{\partial x_j} = \frac{\partial}{\partial x_j} \left( \left( \nu + \frac{\nu_t}{\sigma_k} \right) \frac{\partial k}{\partial x_j} \right) + P_k - \varepsilon \quad (4)$$

$$\frac{\partial \varepsilon}{\partial t} + \frac{\partial [\bar{u}_j \varepsilon]}{\partial x_j} = \frac{\partial}{\partial x_j} \left( \left( \nu + \frac{\nu_t}{\sigma_\varepsilon} \right) \frac{\partial \varepsilon}{\partial x_j} \right) + C_{\varepsilon 1} P_k \frac{\varepsilon}{k} - C_{\varepsilon 2} \frac{\varepsilon^2}{k} \quad (5)$$

where,  $P_k$  is the production (or) generation of turbulent kinetic energy as follows,

$$P_k = \nu_t S^2 \quad \text{where,} \quad S = \sqrt{\frac{1}{2} \left[ \frac{\partial \bar{u}_i}{\partial x_j} + \frac{\partial \bar{u}_j}{\partial x_i} \right]^2} \quad (6)$$

$$\nu_t = c_\mu \frac{k^2}{\varepsilon} \quad (7)$$

The constants for the standard model adopted in the aforementioned equations are:  $C_\mu = 0.09$ ,  $C_{\varepsilon 1} = 1.44$ ,  $C_{\varepsilon 2} = 1.92$ ,  $\sigma_k = 1.0$  and  $\sigma_\varepsilon = 1.3$ . Detailed descriptions on various turbulence models are given in Launder and Sharma [13].

### 2.2 Initial and Boundary Conditions

The flow domain for the present study is shown in Fig. 1. The boundary conditions are as follows:

- Inlet - uniform velocity of  $U$
- Outlet - constant pressure
- Square obstacle wall and side walls- No-slip

### 2.3 Solution Algorithms

The governing equations have been solved by finite volume method with a general purpose CFD code. PISO algorithm was implemented for Pressure-velocity coupling. The first order upwind scheme were implemented to combine the convective and diffusive fluxes. Implicit time marching procedure with time step ( $\Delta t$ ) determined by the CFL (Courant–Friedrichs–Lewy) condition has been implemented for temporal part. CFL criterion was used for the discrete temporal step  $\Delta t$ . convergence criteria is set to absolute error,  $\varepsilon < 10^{-4}$ .

### 3. Results and discussion

#### 3.1.1. Simulation of flow following a square obstacle

The domain size is adopted from Bosch and Rodi [32] as shown in Fig. 1.

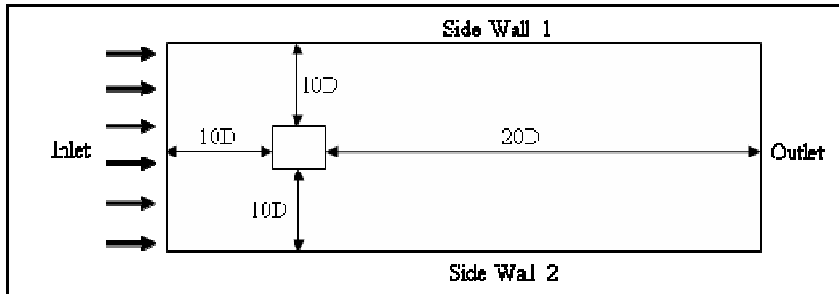


Fig. 1. Computational domain

#### 3.1.2. Grid Independence Test

In any CFD simulation, the dependence of the grids should be checked to rely on the results. Grid independence tests are carried out with three different mesh sizes for  $Re = 2.2 \times 10^4$ . Grids are structured in such a way to have more number of grids closer to the square as shown in Fig. 2 to capture the lift and drag. Different mesh sizes adopted for the grid sensitivity study are shown in Table 1. The force coefficients, Strouhal number, CPU time requirements associated with grid sizes are presented. The difference in the results attained with mesh M2 and M3 is very small, thus M2 is employed for further study. Fig. 3 shows the time variations with the drag force coefficients for the three different mesh sizes. Increase in the number of cells reduces the mean drag coefficient value (Fig. 3).

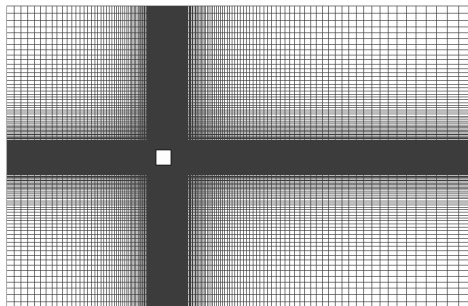


Fig. 2. Global grid pattern

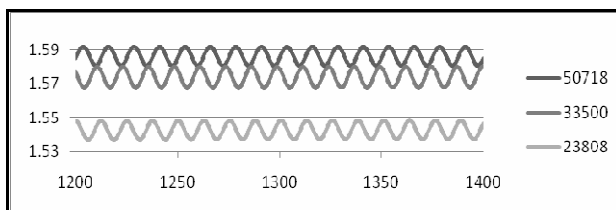


Figure 3. Drag coefficient of mesh M1, M2, and M3

Table-1: Grid Independence Test

Re = 22000					
No. of case	Mesh	No. of elements	$C_D$	St	CPU time per 1000 iteration (sec)
1	M1	23808	1.543	0.124	1140
2	M2	33500	1.574	0.123	1210
3	M3	50718	1.587	0.124	1290

### 3.1.3. Transient wake characteristics

The spatio-temporal variations of the wake behind the square obstacle is examined using a mesh of size M2 with blockage ratio ( $\beta$ ) is kept as 7% and compared with the results of Bosch and Rodi [32]. This grid size is selected after carrying out detailed grid independence study. The variation in the fluid flow at different times are presented in Fig. 4. Here, using streamline contours, the onset of vortex shedding and alternate nature of vortex shedding are well captured. In the adverse pressure gradient region behind the square obstacle, the fore and after symmetry is lost as in Fig. 4(a), due to percolation of viscous effects. Further circulation from the upstream shear layers lead to flow separation and two small attached eddies are formed behind the body as in Fig. 4(b). This pair of symmetric attached eddies grow in size as a function of time up to a size of about 5D as in Fig. 4(c). Subsequently, symmetry is triggered as can be seen in Fig. 4(d), when the standing eddies cease to gain further strength. This is the point at which vortex shedding inception starts. One cycle of vortex shedding is complete, when two eddies of the opposite vorticity are shed. However, when the eddy shedding process is well established and organized, the eddy formation is closer, tighter and confined to approximately the size of the cylinder diameter as shown in Fig. 4(e) and 4(f). Vorticity contours at time T=2400 sec are compared in Fig. 5.

**Table 2. Drag coefficient and Strouhal number compared with other numerical studies**

Author	Turbulence model	$C_D$	St
Kato and Launder	Standard k- $\epsilon$ model	1.660	0.127
Bosch	Standard k- $\epsilon$ model	1.618	0.126
Present	Standard k- $\epsilon$ model	1.627	0.124

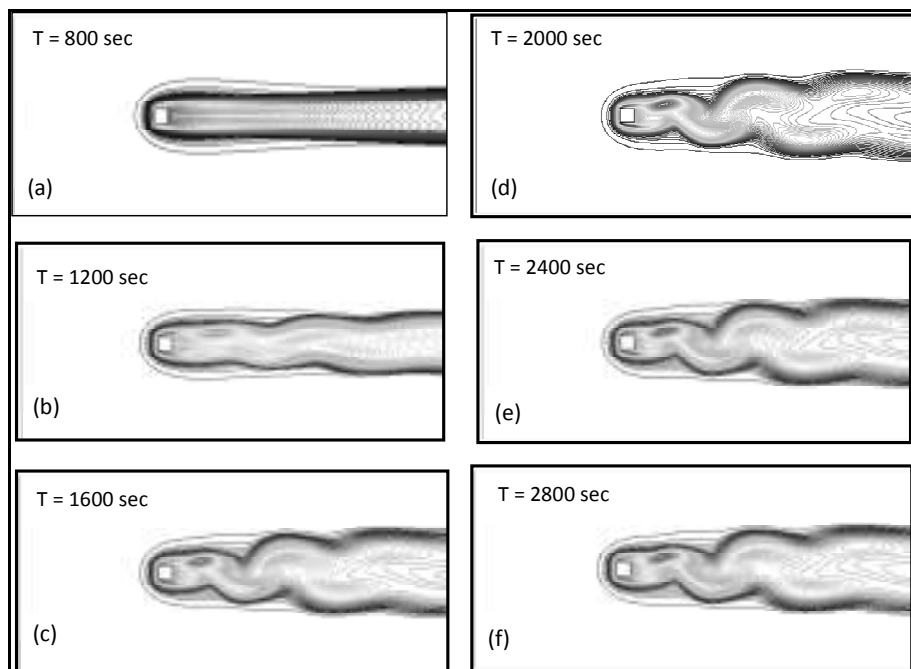


**Fig. 4. Streamline contours at different time**

### 3.1.4. Transient flow characteristics

The lift and drag forces are acquired by incorporating the normal & tangential stresses owing to the gradients of pressure and velocity. The temporal evolutions of ' $C_D$ ' and the ' $St$ ' on the obstacle are available in Table – 3 for different turbulence models. The value of drag force are in a close range for SST k- $\omega$  and Kato-Launder model as compared to other turbulence models whereas the value of ' $St$ ' is over predicted by the latter.

The non-dimensional vorticity distribution near the cylinder is shown in Fig.5. for the different turbulence models at T=2400 sec. The difference in the cases are observed for the same phase angle. The vortices initiating at leading edges of obstacle are stronger and eventually lead to wakes. The shear layer gets separated near the square obstacle for standard k- $\omega$  where as it take a longer path for other turbulence models.

The standard k-ε model reveals extended vortices but the centers of the disconnected vortices stay on their side with respect to the cylinder centerline which is not observed in other models.

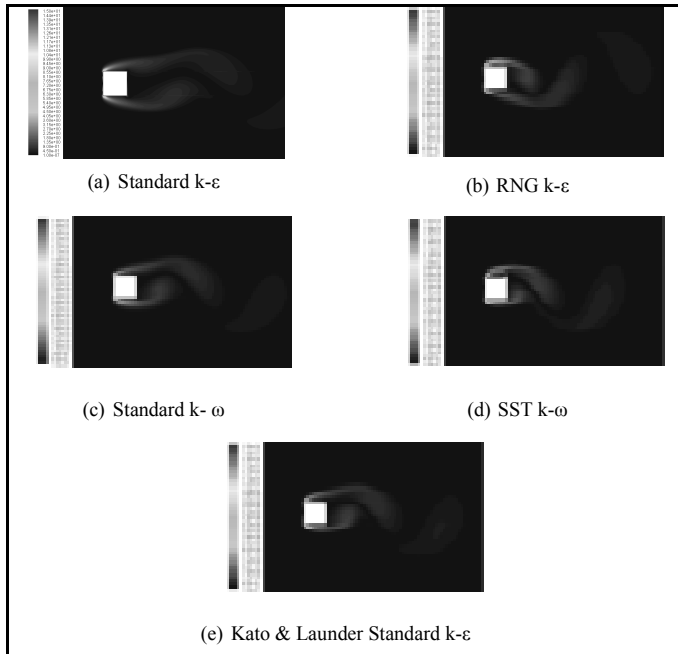


Fig.5 .Calculated distribution of the vorticity at time = 2400 sec

Table 3. Drag coefficient and Strouhal number of different turbulence model

Turbulence model	$C_D$	St
Standard k-ε	1.627	.124
RNG k-ε	1.965	.133
Standard k-ω	2.032	.126
SST k-ω	1.865	.129
Kato & Launder Standard k-ε	1.845	.134

In Fig.6 the time mean turbulent kinetic energy  $k/u_\infty^2$  for different turbulence models at  $y=0$  on the symmetry line is shown. When compared to the surroundings of the symmetry line, 'k' is lesser at the symmetry line. The peak values of the non-dimensional 'k', were observed at the downstream of the obstacle with significant variation in the maximum values of  $k/u_\infty^2$  for different models.

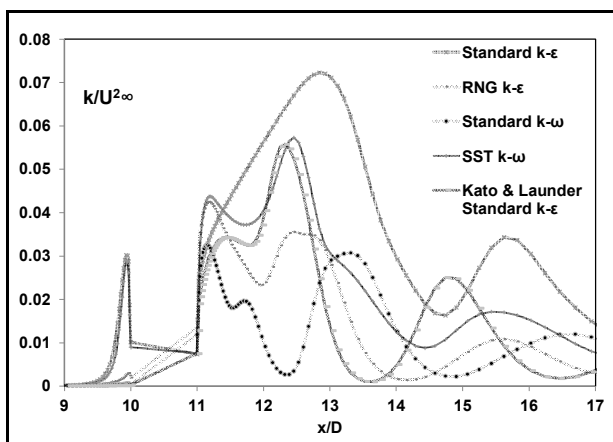
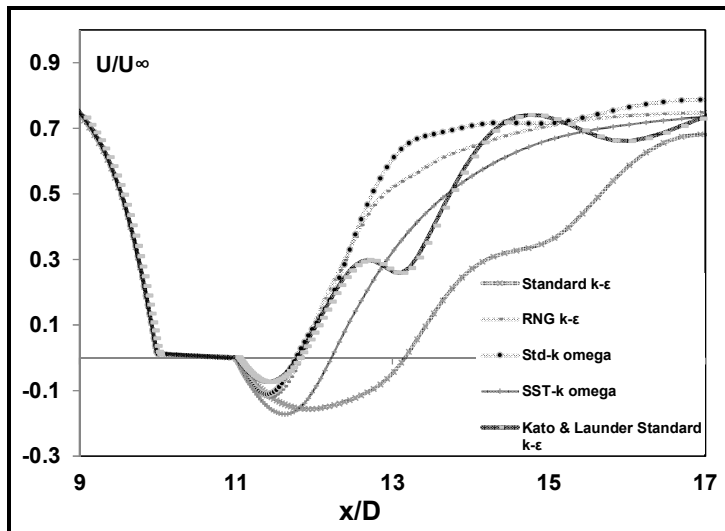


Fig. 6:Non dimensional velocity component distribution on the symmetry line at the centre of the obstacle with different turbulence models.

The distribution of the non-dimensional velocity component  $u/u_{\infty}$  on the obstacle center line is shown in Fig.7. A prominent recirculation zone is evident from the use of standard  $k-\epsilon$  model (Fig. 7). Therefore, with the above mentioned turbulence modeling strong periodic shedding appears due to the small time-averaged recirculation zone (Fig.7).



**Fig.7. Non dimensional velocity component distribution on the symmetry line at the centre of the cylinder with different turbulence models.**

#### 4. Conclusion

The  $k-\epsilon$  turbulence model produced superior results as compared to other turbulence models. The less production of the turbulence in front of the square obstacle resulted in the low turbulence sweeping around the edges. The statistical turbulence model underestimates the turbulent kinetic energy. The use of the  $k-\epsilon$  model predicts experimental observation reasonably well.

#### References

1. Rajan KS. Validation of a one-dimensional, two-fluid model for prediction of hydrodynamics and gas-solid heat transfer in pneumatic conveying. *Int J ChemTech Res* 2013;5:1558–65.
2. Rajan KS. Simulation of vertical gas-solid flow: Comparison of correlations for particle-wall friction and drag coefficient. *Int J ChemTech Res* 2012;4:1234–321.
3. Rajan KS. Simulation of pneumatic drying: Influence of particle diameter and solid loading ratio. *Int J ChemTech Res* 2012;4:1633–41.
4. Rajan KS, Srivastava SN, Pitchumani B, Mohanty B. Simulation of countercurrent gas-solid heat exchanger: Effect of solid loading ratio and particle size. *Appl Therm Eng* 2007;27:1345–51.
5. Rajan KS, Pitchumani B, Srivastava SN, Mohanty B. Two-dimensional simulation of gas-solid heat transfer in pneumatic conveying. *Int J Heat Mass Transf* 2007;50:967–76.
6. Rajan KS, Srivastava SN, Pitchumani B, Mohanty B. Simulation of gas-solid heat transfer during pneumatic conveying: Use of multiple gas inlets along the duct. *Int Commun Heat Mass Transf* 2006;33:1234–42.
7. Bearman P. W. TDM. An investigation of the flow around rectangular cylinders. *Aeronaut Q* 1972;23:229–37.
8. Bearman PW. Near wake flows behind two- and three-dimensional bluff bodies. *J Wind Eng Ind Aerodyn* 1997;69-71:33–54.
9. Iaccarino G, Ooi a., Durbin P a., Behnia M. Reynolds averaged simulation of unsteady separated flow. *Int J Heat Fluid Flow* 2003;24:147–56.
10. Johansen ST, Wu J, Shyy W. Filter-based unsteady RANS computations. *Int J Heat Fluid Flow* 2004;25:10–21.
11. Kawashima N, Kawamura H. Numerical Analysis of Les of Flow Past a Long Square Cylinder. *Proc ERCOFTAC Work* 1996;5:413–22.

12. Knisely CW. Strouhal Numbers of Rectangular Cylinders At Incidence: A Review And New Data. *J Fluids Struct* 1990;371–93.
13. Launder B.E, Sharma I.B. Application of the energy-dissipation model of turbulence to the calculation of flow near a spinning disc. *Int Commun Heat Mass Transf* 1974;1:131–7.
14. Norberg C. Flow around rectangular cylinders: Pressure forces and wake frequencies. *J Wind Eng Ind Aerodyn* 1993;49:187–96.
15. Okajima a. Numerical simulation of flow around rectangular cylinders. *J Wind Eng Ind ...* 1990;33:171–80.
16. Perumal DA, Kumar GVS, Dass AK. Numerical Simulation of Viscous Flow over a Square Cylinder Using Lattice Boltzmann Method. *ISRN Math Phys* 2012;2012:1–16.
17. Sohankar a., Norberg C, Davidson L. Numerical simulation of unsteady low-Reynolds number flow around rectangular cylinders at incidence. *Doktorsavhandlingar Vid Chalmers Tek Hogsk* 1998;71:189–201.
18. Sohankar a, Davidson L, Norberg C. Numerical Simulation of unsteady Flow around A square Two-Dimensional Cylinder. *Twelfth Australas Fluid Mech Conf* 1995:517.
19. Tetsuro T, Kuwahara K. Numerical study of aerodynamic behavior of a square cylinder. *J Wind Eng Ind Aerodyn* 1990;33:161–70.
20. Versteeg HK, Malalasekera W. *An introduction to computational fluid dynamics: the finite volume method.* 2007.
21. Shi LL, Liu YZ, Sung HJ. On the wake with and without vortex shedding suppression behind a two-dimensional square cylinder in proximity to a plane wall. *J Wind Eng Ind Aerodyn* 2010;98:492–503.
22. Lam K, Lin YF, Zou L, Liu Y. Numerical study of flow patterns and force characteristics for square and rectangular cylinders with wavy surfaces. *J Fluids Struct* 2012;28:359–77.
23. Minguez M, Brun C, Pasquetti R, Serre E. Experimental and high-order LES analysis of the flow in near-wall region of a square cylinder. *Int J Heat Fluid Flow* 2011;32:558–66.
24. Lankadasu a., Vengadesan S. Onset of vortex shedding in planar shear flow past a square cylinder. *Int J Heat Fluid Flow* 2008;29:1054–9.
25. Yen SC, Yang CW. Flow patterns and vortex shedding behavior behind a square cylinder. *J Wind Eng Ind Aerodyn* 2011;99:868–78.
26. Chen JM, Liu CH. Vortex shedding and surface pressures on a square cylinder at incidence to a uniform air stream. *Int J Heat Fluid Flow* 1999;20:592–7.
27. Chatterjee D, Mondal B. Effect of thermal buoyancy on vortex shedding behind a square cylinder in cross flow at low Reynolds numbers. *Int J Heat Mass Transf* 2011;54:5262–74.
28. Straatman AG, Martinuzzi RJ. An examination of the effect of boundary layer thickness on vortex shedding from a square cylinder near a wall. *J Wind Eng Ind Aerodyn* 2003;91:1023–37.
29. Shi LL, Liu YZ, Wan JJ. Influence of wall proximity on characteristics of wake behind a square cylinder: PIV measurements and POD analysis. *Exp Therm Fluid Sci* 2010;34:28–36.
30. Lyn DA, Rodi W. The flapping shear layer formed by flow separation from the forward corner of a square cylinder. *J Fluid Mech* 2006;267:353.
31. Raisee M, Jafari A, Babaei H, Iacovides H. Two-dimensional prediction of time dependent, turbulent flow around a square cylinder confined in a channel. *Int J Numer Methods Fluids* 2009:n/a – n/a.
32. Bosch G, Rodi W. Simulation of vortex shedding past a square cylinder with different turbulence models. *Int J Numer Methods Fluids* 1998;28:601–16.
33. Patankar S.V. *Numerical heat transfer and fluid flow.* 1980.

\*\*\*\*\*